

Vibrational Resonance in Time-Delayed Nonlinear Systems

S. Rajasekar and M.A.F. Sanjuán

Abstract Time-delay is ubiquitous in many dynamical systems. The role of single and multiple time-delay on vibrational resonance in a single Duffing oscillator and in a system of n Duffing oscillators coupled unidirectionally and driven by both a low- and a high-frequency periodic force is presented. The investigation is performed through both theoretical approach and numerical simulation. Theoretically determined values of the amplitude of the high frequency force and the delay-time at which resonance occurs are in very good agreement with the numerical simulation. A major consequence of time-delay feedback is that it gives rise to a periodic or quasiperiodic pattern of vibrational resonance profile with respect to the time-delay parameter. For the system of n -coupled oscillators with a single time-delay coupling, the response amplitudes of the oscillators are shown to be independent of the time-delay. In the case of a multi time-delayed coupling, undamped signal propagation occurs for coupling strength (δ) above a certain critical value (denoted as δ_u). Further, the response amplitude approaches a limiting value Q_L with the oscillator number i . Analytical expressions for both δ_u and Q_L are determined.

1 Introduction

Signal detection and signal amplification are very important in engineering, physics and biology. In recent years certain nonlinear phenomena are explored in this

S. Rajasekar

Nonlinear Dynamics, Chaos and Complex Systems Group, Departamento de Física, Universidad Rey Juan Carlos, Tulipán s/n, 28933 Móstoles, Madrid, Spain
e-mail: rajasekar@cnld.bdu.ac.in; srj.bdu@gmail.com

M.A.F. Sanjuán (✉)

Nonlinear Dynamics, Chaos and Complex Systems Group, Departamento de Física, Universidad Rey Juan Carlos, Tulipán s/n, 28933 Móstoles, Madrid, Spain
e-mail: miguel.sanjuana@urjc.es

context. Particularly, certain resonance dynamics are shown to be useful for weak signal detection. Examples include stochastic resonance [1, 2], chaotic resonance [3], coherence resonance [4] and vibrational resonance (VR) [5]. In the case of stochastic resonance a bistable or an excitable system is driven by a weak periodic signal and noise. When the noise intensity is varied the signal-to-noise ratio (SNR) at the frequency of the input periodic signal becomes maximum at an optimum value. On either side of the optimum value of the noise intensity the SNR decreases. In place of noise one can use a chaotic signal of a system. The resulting resonance is called chaotic resonance. It is possible to realize a noise-induced resonance in the absence of the external periodic force and then is termed coherence resonance.

In the VR set-up, a nonlinear system is driven by a biharmonic force consisting of two frequencies ω and Ω with $\Omega \gg \omega$. In a typical VR, when the amplitude (or frequency) of the high-frequency force is varied, the response amplitude of the system at the low-frequency ω displays one or more resonance peaks. VR can occur even in overdamped single-well systems. Theoretical approaches have been developed to analyse VR [6, 7]. VR has been studied in monostable [8], bistable [5–7, 9, 10], three well [11] and spatially periodic potential [12] systems. It has also been observed in excitable systems [13], fractional-order systems [14], maps [15], small-world networks of FitzHugh–Nagumo equations [16] and ecological systems [17]. VR is found to induce undamped low-frequency signal propagation in one-way coupled [18] and globally coupled [19] bistable systems. Experimental evidence of VR has been demonstrated in analog simulations of the overdamped Duffing oscillator [9], in an excitable electronic circuit with Chua’s diode [13] and in a bistable optical cavity laser [20].

It is important to study VR in different kinds of systems and explore its features with specific emphasis on the development of theoretical analysis and the role of properties of the systems on VR. This is precisely what motivates us to consider here a class of dynamical systems called time-delayed systems. When the state of a system at time t depends on its state at a shifted earlier time, say, $t - \alpha$, then a time-delayed feedback term is introduced in the equation of motion of the system. The study of time-delayed systems has received a great interest in recent years because time-delay is ubiquitous in many systems [21, 22]. The common sources of time-delay are finite propagation time of transport of information and energy, finite reaction times, memory effects and finite switching speed of amplifiers. Time-delay is easily amenable in networks [23], laser arrays [24–26], electronic circuits [27], neural systems [28–30] and optical and optoelectronic circuits. The features of vibrational resonance in the presence of a single time-delayed feedback have been analysed in the Langevin equation [31], two-coupled overdamped anharmonic oscillators [32], underdamped and overdamped Duffing oscillators [33], FitzHugh–Nagumo neuronal model [34], a genetic toggle-switch [35] and a system of n -coupled bistable oscillators [36]. There are some notable reports on the influence of two or three time-delayed feedbacks or coupling terms [37–44] on the dynamics of certain systems.

Motivated by the above ideas, here we present our investigation on the effect of single and multi time-delayed feedback (MTDF) on VR in a single nonlinear system

and signal transduction in a system of unidirectionally coupled systems with multi time-delayed coupling (MTDC). We choose the paradigmatic Duffing oscillator as the reference model system. The MTDF is of the form $(\gamma/L) \sum_{l=1}^L x(t-l\alpha)$. $L = 1$ corresponds to a single time-delay. Our main goal is to explore the enhancement of the response amplitude by the single and MTDF and MTDC.

The equation of motion of the single Duffing oscillator with an MTDF and driven by the biharmonic force is given by

$$\ddot{x} + d\dot{x} + \omega_0^2 x + \beta x^3 + \frac{\gamma}{L} \sum_{l=1}^L x(t-l\alpha) = f \cos \omega t + g \cos \Omega t, \quad (1)$$

where $\Omega \gg \omega$. When $d = 0$, $\gamma = 0$, $f = 0$ and $g = 0$ the potential of the Duffing oscillator is $V(x) = \frac{1}{2}\omega_0^2 x^2 + \frac{1}{4}\beta x^4$. For $\omega_0^2 < 0$ and $\beta > 0$ the potential becomes a double-well shape, while for $\omega_0^2 > 0$ and $\beta > 0$ it becomes a single-well form. We treat the double-well and the single-well cases separately. For $f \ll 1$ and because of $\Omega \gg \omega$ it is reasonable to assume that the response of the system (Eq. 1) essentially contains only a slow component $X(t)$ with the low-frequency ω and a fast component $\psi(t, \Omega t)$ with the high-frequency Ω . Through a theoretical approach we obtain an analytical expression for the variables X and ψ . We define the ratio of the amplitude A_L of slow motion and the amplitude f of the input low-frequency force as response amplitude Q . First we analyse the occurrence of VR in the system (Eq. 1) with single time-delay ($L = 1$). From the theoretical expression of Q we determine the values of g and α denoted as g_{VR} and α_{VR} , respectively, at which VR occurs, i.e., Q becomes a maximum. We verify the theoretical predictions with the numerical simulation. We illustrate the mechanism of the resonance and compare the change in the slow motion $X(t)$ and the actual motion $x(t)$ when the control parameters g and α are varied. Next, we analyse the effect of MTDF on VR. We determine the regions in $(\gamma - \alpha)$ parameter space for which $Q_{\text{max}}(\gamma) > Q_{\text{max}}(\gamma = 0)$ for a few fixed values of L . It displays a band-like structure with the number of bands being the number of time-delayed terms L . We analyse the effect of L on resonance.

Then we take up the n -coupled Duffing oscillators whose equations read

$$\begin{aligned} \ddot{x}_i + d\dot{x}_i + \omega_0^2 x_i + \beta x_i^3 &= f \cos \omega t + g \cos \Omega t, \\ \ddot{x}_i + d\dot{x}_i + \omega_0^2 x_i + \beta x_i^3 &= \frac{\delta}{L} \sum_{l=1}^L x_{i-1}(t-l\alpha), \end{aligned} \quad (2)$$

where $i = 2, 3, \dots, n$. Our prime interest is on the analysis of signal propagation in the system (Eq. 2) with $n = 200$. Applying the theoretical treatment used for the system (Eq. 1) we express Q_i in terms of Q_{i-1} except for the first oscillator. When $L = 1$, the analytical expression of Q_i , $i > 1$ is found to be independent of the time-delay parameter α . This implies that the time-delay has no influence on Q_i .

For $i \gg 1$ the theoretical Q_i deviates largely from the numerically computed Q_i . This is because of the neglect of nonlinear terms in the equation of motion of the slow variable $X_i(t)$. Inclusion of nonlinear terms leads to a set of coupled nonlinear equations for Q_i . Interestingly, the Q_i 's computed by solving this set of equations are in very good agreement with the numerically calculated Q_i . The coupled system shows undamped signal propagation (that is, $Q_{200} > Q_1$) for certain range of values of the control parameters α and δ . In the undamped signal propagation, Q_i exhibits sigmoidal type of variation with i , that is, $Q_i \rightarrow Q_L$ for sufficiently large i . We are able to obtain an analytical expression for the limiting value of Q , Q_L , and the critical value of δ , δ_u , above which undamped signal propagation takes place. Interestingly, both Q_L and δ_u are independent of the parameter g .

Before taking up the main theme, in the next two sections we briefly point out that time-delay is ubiquitous and show the absence of VR in a linear system with time-delayed feedback and driven by the biharmonic force.

2 Time-Delay Is Ubiquitous

A first-order delay differential equation is of the form

$$\dot{x} = F(t, x(t), x(t - \alpha_l)), \quad (3)$$

where $\alpha_l > 0$, $l = 1, 2, \dots$ are delay times. The time-delays α_l can be of different types depending upon the nature of the sources of the time-delay. In the nonlinear dynamics literature the effect of the following types of time-delay is investigated in a variety of nonlinear systems [22]:

1. A single constant delay: $\alpha_l = \alpha = \text{a constant}$, $l = 1$.
2. Multiple time-delay: $\alpha_l = l\alpha$, $\alpha = \text{a constant}$, $l = 1, 2, \dots, L$. An example is

$$F(x(t - \alpha_l)) = \frac{1}{L} \sum_{l=1}^L x(t - l\alpha).$$

3. Integrative time-delay or distributive delay: A delay term of this kind is represented as $\langle x \rangle_\alpha = \frac{1}{\alpha} \int_{t-\alpha}^t x(t') dt'$.
4. Time-dependent delay: $\alpha(t) = a + bt$ or $a + b\sqrt{t}$ with $\alpha < t$.
5. State-dependent delay: $\alpha = F(x(t))$. An example is $\alpha(x(t)) = |x(t)|$.

Typical examples of systems with delays are given by maturation times [45], hydrodynamic problems [46], chemical surface reactions [47] and feedback regulated voltage-controlled oscillators [48, 49]. In nonlinear optics, periodic and chaotic outputs are realized by a delayed feedback [50]. Such delay-induced dynamics are used to design practical systems including high-frequency and broadband optical chaotic oscillators for secure chaos communication [51] or high-speed random number generation [52] or to develop alternative imaging techniques [50].

It is noteworthy to mention that delayed self-communication is of great significance because of its regulatory mechanism in nature and technology [53, 54]. Examples include excitable gene regulatory systems [55], eye movements [56], human balance [57] and optically communicating semiconductor lasers [58]. In neural networks communicating between the various areas may take place in delays ranging from few milliseconds to hundreds of milliseconds due to the finite speed of the transfer of data in the axons and dendrites and because of the processing latency in the synapses [59]. In neural systems the source for a precise firing of basket cells in hippocampus during Theta and Gamma rhythm is a delayed feedback. Experimental evidences are reported for delayed recurrent excitations inducing regulation of the structure of the interspike intervals in the presence of noise [60]. Delayed self-coupling in the study of the pacemaker cells of crayfish [61] is found to give rise bursting and high-frequency discharges with relatively long quiescent intervals [62]. One can treat the time-delay as an external force.

In coupled systems, coupling transmits one or more variables to neighbours. Often the transmission time is larger than the internal time scales of the systems. In this case coupling terms consisting of time-delayed variables are realistic. Message decoding in chaos-based communication systems would require chaos synchronization between multiple time-delayed transmitter and receiver systems. In high speed chaos-based communication systems [63] external cavity semiconductor lasers form an integral part. In practical applications such lasers may be subject to more than one optical reflection. This would lead to multiple time-delays. It has been pointed out that inclusion of several external cavities could provide higher security for such communication systems [64].

3 Resonance in a Linear System with Time-Delayed Feedback

In this section we consider a linear system with linear MTDf and driven by two periodic forces. The equation of motion of the system is given by

$$\ddot{x} + d\dot{x} + \omega_0^2 x + \frac{\gamma}{L} \sum_{l=1}^L x(t - l\alpha) = f \cos \omega t + g \cos \Omega t, \quad (4)$$

where $\omega_0^2 > 0$ and $d > 0$. The general solution of Eq.(4) for $f = g = 0$ is not known. Equation (4) with $f = g = \gamma = 0$ is a damped linear system. Its equilibrium point $(x^*, \dot{x}^*) = (0, 0)$ is stable. When $f = g = 0$ and $\gamma \neq 0$, Eq. (4) exhibits a damped or periodic or growing oscillation depending upon the values of γ , L and α [22]. Here, we are interested in the long time behaviour of Eq. (4). In the limit $t \rightarrow \infty$ we seek the solution of Eq. (4) in the form

$$x(t) = A_\omega \cos(\omega t + \phi_\omega) + A_\Omega \cos(\Omega t + \phi_\Omega). \quad (5)$$

The unknowns A_ω and ϕ_ω are determined as

$$A_\omega = \frac{f}{\sqrt{S_\omega}}, \quad S_\omega = \left[\omega_0^2 - \omega^2 + \frac{\gamma}{L} \sum_{l=1}^L \cos l\alpha\omega \right]^2 + \left[d\omega - \frac{\gamma}{L} \sum_{l=1}^L \sin l\alpha\omega \right]^2, \quad (6)$$

$$\phi_\omega = \tan^{-1} \left[\frac{d\omega - \frac{\gamma}{L} \sum_{l=1}^L \sin l\alpha\omega}{\omega^2 - \omega_0^2 - \frac{\gamma}{L} \sum_{l=1}^L \cos l\alpha\omega} \right]. \quad (7)$$

Replacement of ω and f by Ω and g , respectively, in Eqs. (6) and (7) gives A_Ω , S_Ω and ϕ_Ω . As $f(g)$ increases $A_\omega(A_\Omega)$ also increases. Resonance does not occur at the frequencies ω or Ω when f or g is varied from a small value. Thus, there is no vibrational resonance in the linear system with time-delayed feedback.

4 Single Duffing Oscillator: Theoretical Expression for the Response Amplitude Q

The main objective of this section is to obtain an expression for the response amplitude Q for the single Duffing oscillator system of Eq. (1) [65].

We assume the solution of the system (Eq. 1) for $\Omega \gg \omega$ as $x = X + \psi$ where $X(t)$ and $\psi(\tau = \Omega t)$ are a slow motion with period $2\pi/\omega$ in the time t and a fast motion with period 2π in the fast time τ , respectively. Further, we assume that the average value of ψ over the period 2π is $\langle \psi \rangle = \frac{1}{2\pi} \int_0^{2\pi} \psi \, d\tau = 0$. Substitution of $x = X + \psi$ in Eq. (1) gives the following equations for the variables X and ψ :

$$\begin{aligned} \ddot{X} + d\dot{X} + (\omega_0^2 + 3\beta\langle\psi^2\rangle)X + \beta(X^3 + \langle\psi^3\rangle) + 3\beta X^2\langle\psi\rangle \\ + \frac{\gamma}{L} \sum_{l=1}^L X(t - l\alpha) = f \cos \omega t, \end{aligned} \quad (8)$$

$$\begin{aligned} \ddot{\psi} + d\dot{\psi} + \omega_0^2\psi + 3\beta X^2(\psi - \langle\psi\rangle) + 3\beta X(\psi^2 - \langle\psi^2\rangle) \\ + \beta(\psi^3 - \langle\psi^3\rangle) + \frac{\gamma}{L} \sum_{l=1}^L \psi(\Omega t - l\alpha\Omega) = g \cos \Omega t, \end{aligned} \quad (9)$$

where $\langle\psi^n\rangle = \frac{1}{2\pi} \int_0^{2\pi} \psi^n \, d\tau$. Because ψ is a fast variable we can neglect the nonlinear terms in Eq. (9). In the limit of $t \rightarrow \infty$, referring to the solution of the linear system (Eq. 4) given by Eqs. (5)–(7), we write the solution of Eq. (9) as

$$\psi = \mu \cos(\Omega t + \phi), \quad (10)$$

where $\mu = g/k$,

$$k^2 = \left(\omega_0^2 - \Omega^2 + \frac{\gamma}{L} \sum_{l=1}^L \cos l\alpha\Omega \right)^2 + \left(d\Omega - \frac{\gamma}{L} \sum_{l=1}^L \sin l\alpha\Omega \right)^2 \quad (11)$$

and

$$\phi = \tan^{-1} \left(\frac{d\Omega - \frac{\gamma}{L} \sum_{l=1}^L \sin l\alpha\Omega}{\Omega^2 - \omega_0^2 - \frac{\gamma}{L} \sum_{l=1}^L \cos l\alpha\Omega} \right). \quad (12)$$

For sufficiently large values of Ω we can further approximate the solution (Eqs. 10–12) by dropping the terms ω_0^2 and $d\Omega$. However, in our treatment we keep these terms in the solution. From the above solution we obtain $\langle \psi \rangle = 0$, $\langle \psi^2 \rangle = \mu^2/2$ and $\langle \psi^3 \rangle = 0$. Then Eq. (8) becomes

$$\ddot{X} + d\dot{X} + C_1X + \beta X^3 + \frac{\gamma}{L} \sum_{l=1}^L X(t - l\alpha) = f \cos \omega t, \quad (13)$$

where $C_1 = \omega_0^2 + \frac{3}{2}\beta\mu^2$. When $f = 0$, the equilibrium points of Eq. (13) are

$$X_0^* = 0, \quad X_{\pm}^* = \pm \sqrt{-\frac{C_1 + \gamma}{\beta}}. \quad (14)$$

Slow oscillations occur around these equilibrium points.

Substituting $X = Y + X^*$, where Y is the deviation of the slow motion from X^* , in Eq. (13), we obtain

$$\ddot{Y} + d\dot{Y} + \omega_r^2 Y + 3\beta X^* Y^2 + \beta Y^3 + \frac{\gamma}{L} \sum_{l=1}^L Y(t - l\alpha) = f \cos \omega t. \quad (15)$$

The solution of the linear version of Eq. (15) in the limit $t \rightarrow \infty$ and $f \ll 1$ is $Qf \cos(\omega t + \theta)$, where the response amplitude Q and the phase θ are given by

$$Q = \frac{1}{\sqrt{S}}, \quad S = \left(\omega_r^2 - \omega^2 + \frac{\gamma}{L} \sum_{l=1}^L \cos l\alpha\omega \right)^2 + \left(d\omega - \frac{\gamma}{L} \sum_{l=1}^L \sin l\alpha\omega \right)^2 \quad (16)$$

and $\theta = \phi(\Omega = \omega, \omega_0^2 = \omega_r^2)$. ω_r is the resonant frequency of the linear version of the equation of motion of the slow variable $X(t)$. In the next section we analyse the occurrence of VR in the system (Eq. 2) with a single time-delayed feedback term and then take up the system with MTDF.

5 Resonance in the System with a Single Time-Delay

In the absence of the damping term, external periodic forces and feedback term the potential of the Duffing oscillator is $V(x) = \frac{1}{2}\omega_0^2 x^2 + \frac{1}{4}\beta x^4$. $V(x)$ becomes a double-well for $\omega_0^2 < 0, \beta > 0$, and a single-well for $\omega_0^2, \beta > 0$, respectively. Moreover, for $\omega_0^2 > 0, \beta < 0$ the potential has a single-well with double-hump form. These three forms of the potential are depicted in Fig. 1. For $\omega_0^2, \beta < 0$ the potential has an inverted single-well form. We treat the double-well and single-well cases of the system separately.

5.1 Resonance Analysis in the Double-Well System

The equilibrium points around which slow oscillations take place are given by Eq. (14). There are three equilibrium points for $g < g_c$ where

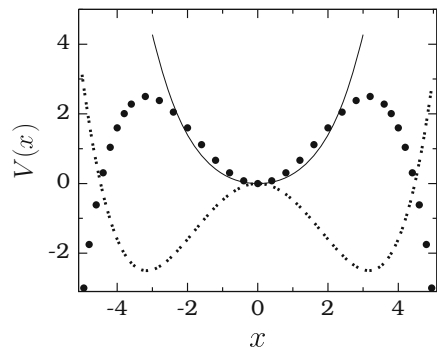
$$g_c = \left[\frac{2k^2}{3\beta} (|\omega_0^2| - \gamma) \right]^{1/2}, \quad |\omega_0^2| - \gamma > 0, \tag{17}$$

For $g < g_c$ the system admits two slow motions, one about X_+^* and the other about X_-^* . X_0^* is unstable. For $g > g_c$, X_0^* is the only real equilibrium point and a slow orbit occurs about it. That is, the effective potential of the slow variable X undergoes a transition from the double-well to a single-well at g_c .

The possibility of occurrence of resonance when a control parameter is varied and the values of a parameter at which resonance occurs can be determined from the theoretical expression of Q . The response amplitude Q is a maximum when the function S in Eq. (16) is a minimum. When a parameter, say, g is varied then resonance occurs at a value of g_{VR} , where g_{VR} is a root of the equation $dS/dg = 0$. This condition requires

$$\omega_r^2 = \omega^2 - \gamma \cos \alpha \omega. \tag{18}$$

Fig. 1 Single-well (represented by a *continuous line*, $\omega_0^2 = 0.5, \beta = 0.1$), double-well (represented by a *dashed line*, $\omega_0^2 = -1, \beta = 0.1$) and single-well with double-hump (represented by *solid circles*, $\omega_0^2 = 1, \beta = -0.1$) forms of the potential of the Duffing oscillator



From this resonance condition one can obtain an analytical expression for g_{VR} . We obtain the following results.

Case 1: $\gamma < 0$

When

$$\gamma < 0, \quad |\gamma| < |\gamma_{c<}| = \frac{\omega^2}{1 - \cos \alpha \omega} \tag{19}$$

there are two resonances. The values of g at which resonance occurs are given by

$$g_{VR}^{(1)} = \left[\frac{k^2}{3\beta} (2|\omega_0^2| - \omega^2 - 3\gamma + \gamma \cos \alpha \omega) \right]^{1/2} < g_c, \tag{20}$$

$$g_{VR}^{(2)} = \left[\frac{2k^2}{3\beta} (|\omega_0^2| + \omega^2 - \gamma \cos \alpha \omega) \right]^{1/2} > g_c. \tag{21}$$

The response amplitude is the same at these two values of g . For $\gamma < 0$ and $|\gamma| > |\gamma_{c<}|$ only one resonance is possible and in this case $g_{VR}^{(1)} = g_c$. For $|\gamma| < |\gamma_{c<}|$ the resonances are due to the matching of ω_r^2 with $\omega^2 - \gamma \cos \alpha \omega$ (refer to Eq. (18)), while the resonance at $g = g_c$ for $|\gamma| > |\gamma_{c<}|$ is due to the local minimization of ω_r^2 .

Case 2: $\gamma > 0$

For $\gamma > 0$, one resonance occurs at $g = g_{VR}^{(2)}$ given by Eq. (21) provided $|\omega_0^2| + \omega^2 > \gamma$. Another resonance occurs at $g = g_{VR}^{(1)}$ given by Eq. (20) if

$$|\omega_0^2| > \gamma, \quad \gamma < \gamma_{c>} = \frac{2|\omega_0^2| - \omega^2}{3 - \cos \alpha \omega}. \tag{22}$$

The two resonances are resulting from the resonance condition (Eq. 18).

To verify the theoretical predictions, we numerically compute the sine and cosine components Q_s and Q_c , respectively, at the low-frequency ω of the numerical solution $x(t)$ of the system (Eq. 1). In the calculation of Q_s and Q_c we use the solution $x(t)$ corresponding to 200 drive cycles of the input signal after leaving a sufficient transient. Then $Q = \sqrt{Q_s^2 + Q_c^2}/f$. We choose the values of the parameters as $d = 0.5$, $\omega_0^2 = -1$, $\beta = 0.1$, $f = 0.1$, $\omega = 1$ and $\Omega = 10$. Equation (1) is integrated numerically using the Euler method with time step 0.01. The time-delay parameter α takes always multiple values of 0.01.

Figure 2a presents both theoretical and numerical g_{VR} as a function of γ for $\alpha = 1$ and 3. We notice a very good agreement between the theory and the numerical simulation. For $\alpha = 1$ and 3 we find $\gamma_{c<} = -2.17534$ and -0.50251 , respectively. For $\gamma < 0$, there are two resonances for $|\gamma| < |\gamma_{c<}|$ and only one for $|\gamma| > |\gamma_{c<}|$. For $|\gamma| < |\gamma_{c<}|$, as g increases from 0 the quantity ω_r^2 decreases from $2|\omega_0^2| + 3|\gamma|$ and reaches the minimum value $|\gamma|$ at $g = g_c$. As g increases from g_c the value

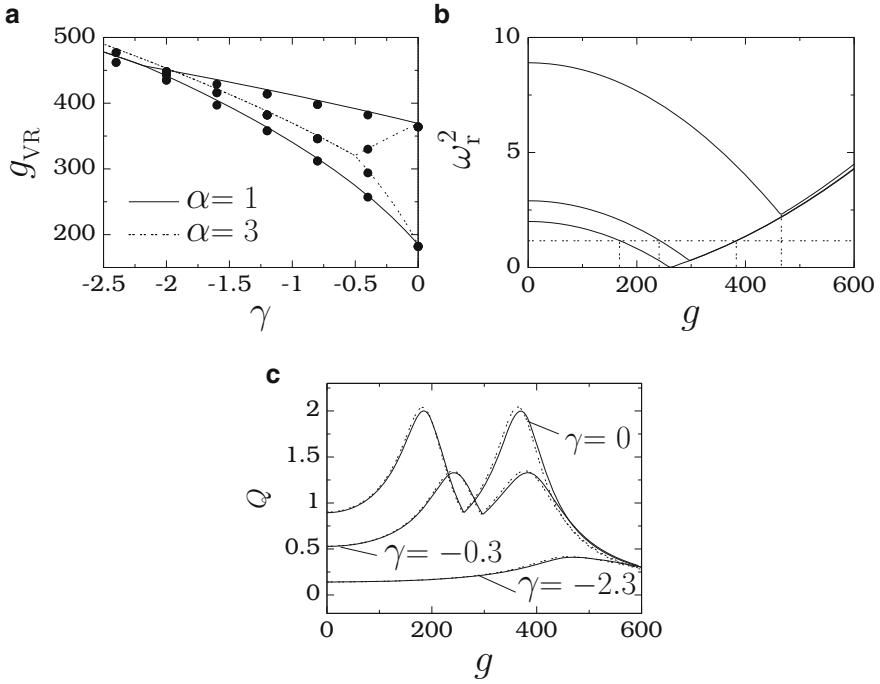


Fig. 2 (a) Theoretical and numerical g_{VR} versus the parameter γ for the system (Eq. 1) with the double-well potential case. The number of delay term is 1. The *solid circles* are the numerically computed g_{VR} and the *lines* are theoretical g_{VR} . (b) ω_r^2 versus g . From *bottom to top* curves the values of γ are 0, -0.3 and -2.3 , respectively. The *horizontal dashed line* represents the value of $(\omega^2 - \gamma \cos \alpha \omega)$. The *vertical dashed lines* mark the values of g_{VR} . (c) Q as a function of g with $\alpha = 1$. The *continuous lines* are theoretical Q while the *dashed lines* are numerically calculated Q

of ω_r^2 increases from $|\gamma|$. This is shown in Fig. 2b for $\gamma = 0, -0.3$ and -2.3 . For $\gamma = 0$ and -0.3 at $g_{VR}^{(1)}$ and $g_{VR}^{(2)}$ we have $\omega_r^2 = \omega^2 - \gamma \cos \alpha \omega$ (indicated by the horizontal dashed line in Fig. 2b) and hence Q becomes maximum with $Q_{max} = 1/|d\omega - \gamma \sin \alpha \omega|$. In Fig. 2c we observe two resonances. In the absence of time-delay feedback Q becomes maximum when $\omega_r = \omega$ and the maximum value of Q is $1/(d\omega)$. For $\gamma = -0.3$ the theoretical values of $g_{VR}^{(1)}$ and $g_{VR}^{(2)}$ are 242.75 and 382.95, while the numerically computed values are 240.34 and 377.43, respectively. For $|\gamma| > |\gamma_{c<}|$ the value of ω_r^2 is always $> (\omega^2 - \gamma \cos \alpha \omega)$. However, it has a local minimum at $g = g_c$ and thus a resonance. These are shown in Fig. 2b,c for $\gamma = -2.3$. Note that Q is minimum at $g = g_c$ for $|\gamma| < |\gamma_{c<}|$.

In Fig. 2c the value of Q at resonance is always lower than the case $\gamma = 0$. $Q_{max}(\gamma, g) = Q(\gamma, g_{VR}) > Q(\gamma = 0, g_{VR})$ can be realized for a range of values of α and γ . Figure 3a presents the variation of $Q(g_{VR})$ in (γ, α) parameter space for $\omega = 1$ and $\gamma < 0$. We can clearly see that $Q(\gamma, g_{VR}) > Q(\gamma = 0, g_{VR})$ for $\alpha \in [\pi, 2\pi]$. Figure 3b is the three-dimensional plot of Q as a function of γ and g

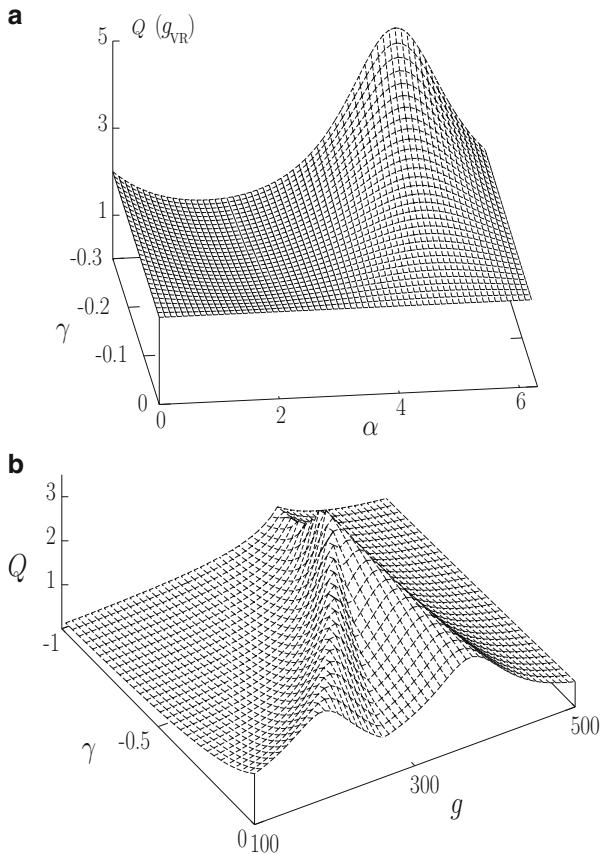


Fig. 3 (a) Variation of $Q(g = g_{VR})$ as a function of γ and α for the double-well case of the system (Eq. 1) with single time-delay. (b) Three-dimensional plot of Q versus the parameters γ and g for $\alpha = 3.5$

for $\alpha = 3.5$. For $\alpha = 3.5$ the value of $|\gamma_{c<}|$ is 0.51641. In Fig. 3b for $|\gamma| < 0.51641$ there are two resonances with $Q(\gamma, g_{VR}) > Q(\gamma = 0, g_{VR})$. Only one resonance occurs for $|\gamma| > 0.51641$.

Now we compare the change in the slow motion $X(t)$ and the actual motion $x(t)$ when the parameter g is varied. For $\gamma = -0.3$ and $\alpha = 1$ the numerically computed values of g_{VR} are 240.5 and 376.85. The phase portrait of slow motion is plotted in Fig. 4 for several values of g . For $g < g_c (= 296.95)$ there are two slow motions: one around X_+^* and the other around X_-^* . As g increases from a small value the equilibrium points about which $X(t)$ and $x(t)$ occur move towards the origin. This is shown in Fig. 4 for four values of $g < g_c$. In this figure the orbits coexisting around X_-^* are not shown for clarity. For $g > g_c$, as noted earlier, $X_0^* = 0$ is the only equilibrium point and hence both $X(t)$ and $x(t)$ occur around the origin. This is evident in Fig. 4 for three values of $g > g_c$. We observe that at the resonance

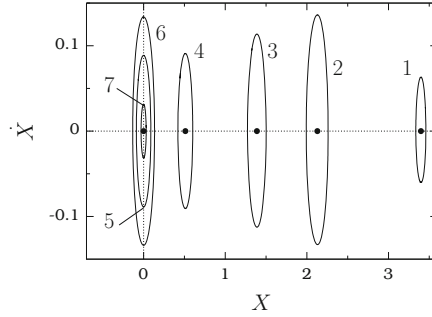


Fig. 4 Phase portraits of the slow variable X of the double-well system (Eq. 1) with single time-delay for several values of g . The values of g for the numbers 1–7 are 100 (1), 240.5 (2), 275 (3), 295 (4), 300 (5), 376.85 (6) and 600 (7). Here $d = 0.5, \omega_0^2 = -1, \beta = 0.1, \gamma = -0.3, \alpha = 1, f = 0.1, \omega = 1$ and $\Omega = 10$. The equilibrium points X_0^* and X_+^* are marked by the *solid circles*

($g = 240.50$) both $x(t)$ and $X(t) > 0$. That is, cross-well motion and bistability are not necessary ingredients for VR. As a matter of fact, it can occur in monostable systems [8].

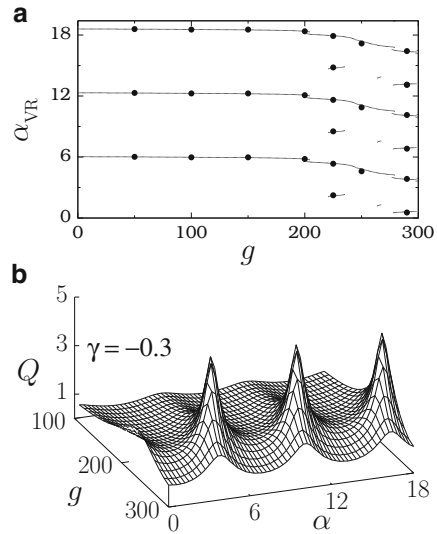
Next, we present the effect of the time-delay parameter α on VR. The condition for a resonance to occur when α is varied is given by (from $dS/d\alpha = 0$)

$$(\omega_r^2 - \omega^2) \omega_{rx}^2 + (\omega_{rx}^2 - d\omega^2) \gamma \cos \alpha\omega - \gamma\omega (\omega_r^2 - \omega^2) \sin \alpha\omega = 0, \quad (23)$$

where $\omega_{rx}^2 = d\omega_r^2/d\alpha$. Analytical expressions for the roots of the above equation are difficult to obtain. However, the roots denoted as α_{VR} can be determined numerically from Eq. (23). We compute theoretical α_{VR} (from Eq. (23)) and numerical α_{VR} (by numerically solving the Eq. (2)) for a range of values of g with $\gamma = -0.3$. In Fig. 5a $\alpha_{VR} < 3 \times 2\pi/\omega$ are alone plotted. (α_{VR} are periodic with period $2\pi/\omega$). Figure 5b presents numerical Q as a function of α and g . We can clearly see the periodicity of Q with respect to α .

Figure 6 illustrates the effect of α on the slow motion $X(t)$ for $g = 250$ and 350 . When α is increased from a small value with $g < g_c$, then the shift in the locations of X_{\pm}^* is very small. However, the amplitude of the slow orbits varies and resonance occurs at $\alpha = \alpha_{VR}$. When α is varied for $g > g_c$ then the slow orbit occurs about $X_0^* = 0$. These are shown in Fig. 6 for $g = 250 < g_c$ and $g = 350 > g_c$. For $g = 250 (< g_c)$ the slow motion occurs about X_+^* and X_-^* . This is shown in Fig. 6a, b for a few fixed values of α . In these figures the resonant orbits are marked by the label 2. The orbits marked by 1 and 3 correspond to the values of α on either side of $\alpha = \alpha_{VR}$. In Fig. 6c,d, for $g = 350 > g_c$ slow motion occurs about $X_0^* = 0$. Tuning time-delay is an advantage when it is desired to observe the response of a system and VR with the centre of the orbit (slow as well as the actual orbit) almost remains the same.

Fig. 5 (a) α_{VR} versus the amplitude g of the high frequency force for $\gamma = -0.3$. The system is the double-well single system. *Continuous lines and painted circles* represent theoretically and numerically computed values of α_{VR} , respectively. (b) Periodic variation of the response amplitude Q with the time-delay parameter α for various values of g in the interval $[100, 300]$ for $\gamma = -0.3$



5.2 Resonance Analysis in the Single-Well System

For $\omega_0^2, \beta > 0$ the potential $V(x)$ of the system has a single-well shape with a local minimum at $x = 0$. Unlike the double-well system, the effective potential of X remains as a single-well when the amplitude g of the high-frequency force is varied. Consequently, slow oscillation always occurs about $X_0^* = 0$.

For the single-well case the resonance value of g is given by

$$g_{VR} = \left[\frac{2k^2}{3\beta} (\omega^2 - \omega_0^2 - \gamma \cos \alpha \omega) \right]^{1/2}. \tag{24}$$

We recall that in the double-well case a resonance is possible for all set of values of γ and α when g is varied. In contrast to this, in the single-well system a resonance is possible only for a set of values of γ and α for which $\omega^2 - \gamma \cos \alpha \omega > \omega_0^2$. Further, in the double-well system two resonances are possible while in the single-well system at most one resonance is possible.

In Fig. 7a we plot the variation of theoretical g_{VR} with γ and α for $\omega_0^2 = 0.5$ and $\beta = 0.1$. For a fixed value of γ as α increases from zero the value of g_{VR} increases and becomes maximum at $\alpha = \pi/\omega$ and then decreases. g_{VR} is periodic in α with period $2\pi/\omega$ and $Q_{max} = 1/|d\omega - \gamma \sin \alpha \omega|$. In Fig. 7b the maximum value of Q at $g = g_{VR}$ for $\alpha = 2$ increases when γ increases. For a certain range of values of α , g_{VR} decreases when γ increases and the value of Q at resonance increases. For example, when $\alpha = 1$ the value of g_{VR} decreases when γ increases. For $\alpha = 2$ and 3 , g_{VR} increases when γ increases.

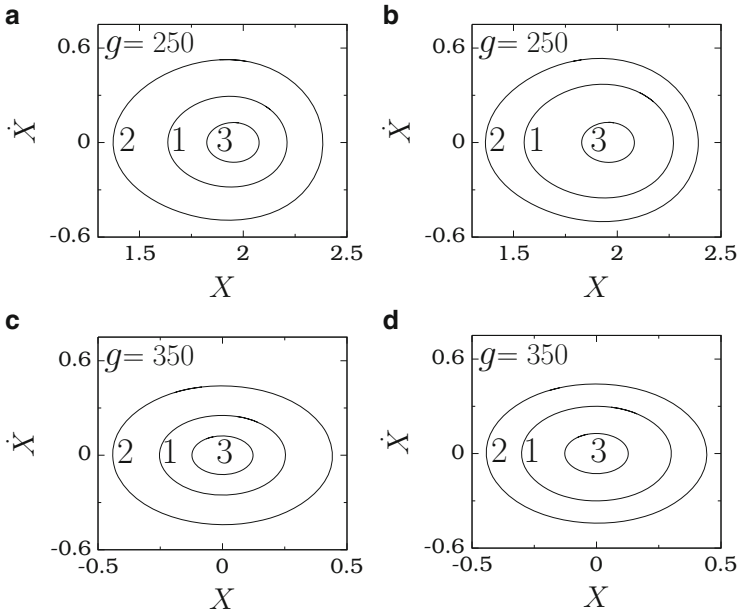


Fig. 6 X versus \dot{X} as a function of $\alpha (\leq 14)$ for two fixed values of g . **(a)** $g = 250$, $\alpha = 4$ (1), 4.57 (2) and 8 (3). **(b)** $g = 250$, $\alpha = 10.5$ (1), 10.97 (2) and 14 (3). **(c)** $g = 350$, $\alpha = 3.5$ (1), 4.41 (2) and 7 (3). **(d)** $g = 350$, $\alpha = 10$ (1), 10.69 (2) and 13 (3). Resonance occurs at $\alpha = 4.57$ and 10.97 for $g = 250$ and at $\alpha = 4.41$ and 10.69 for $g = 350$

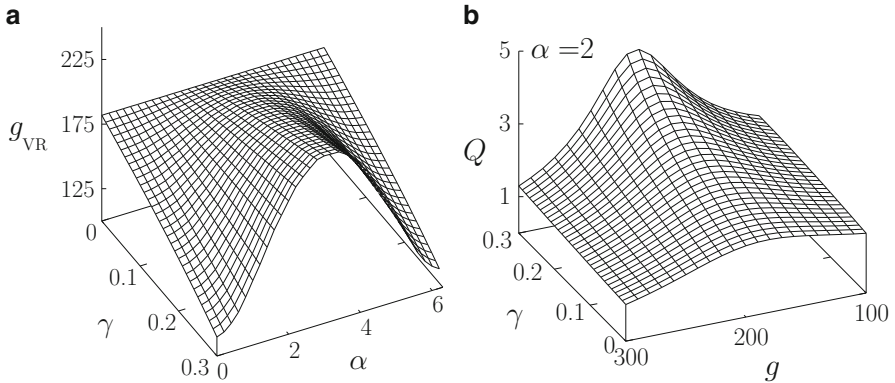
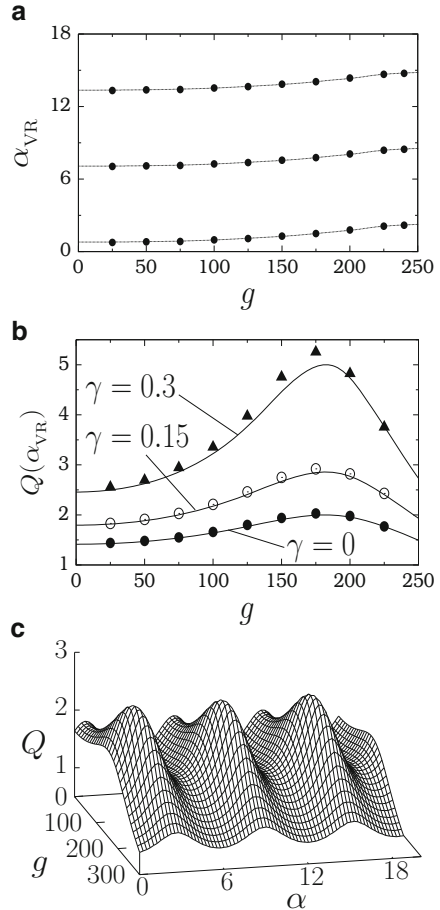


Fig. 7 **(a)** Theoretical g_{VR} versus the time-delay feedback parameters γ and α for the single-well case of the system (Eq. 1) with $L = 1$, $\omega_0^2 = 0.5$ and $\beta = 0.1$. **(b)** Q versus the parameters γ and g for $\alpha = 2$

Figure 8a presents both theoretical and numerical α_{VR} versus g for $\gamma = 0.15$. α_{VR} is periodic with period $2\pi/\omega$. For a fixed value of g resonance occurs at only one value of α for $\alpha \in [0, 2\pi/\omega]$. In Fig. 5a, corresponding to the double-well system, a double resonance is found for a certain range of fixed values of g . The presence

Fig. 8 (a) α_{VR} versus g for $\gamma = 0.15$. The system is the single-well case of Eq. (2) with single delay-time. *Continuous lines* and *solid circles* are the theoretically determined and numerically computed values of α_{VR} , respectively. (b) $Q(\alpha_{VR})$ versus g for three values of γ . (c) Periodic variation of Q with α for various values of g for $\gamma = 0.15$



of only one resonance in Fig. 8a for $\alpha \in [0, 2\pi/\omega]$ implies that the variation of k^2 due to the terms $\gamma \sin \alpha\Omega$ and $\gamma \cos \alpha\Omega$ (see Eq. (11)) is negligible and $k^2 \approx (\omega_0^2 - \Omega^2)^2 + d^2\Omega^2$. Then from Eq. (16) the expression for α_{VR} is obtained as

$$\alpha_{VR} = \frac{1}{\omega} \tan^{-1} \left(\frac{d\omega}{\omega^2 - \omega_r^2} \right), \quad \omega_r^2 = C_1. \tag{25}$$

α_{VR} is independent of γ ; however, the maximum value of Q at resonance varies with γ . This is confirmed in the numerical simulation. The maximum value of Q for $\gamma \neq 0$ is always found to be greater than the value of Q for $\gamma = 0$ (see Fig. 8b). Figure 8c demonstrates the periodic variation of Q with the delay parameter α . For irrational values of the ratio Ω/ω the response amplitude exhibits a quasiperiodic pattern.

6 Single Duffing Oscillator: Effect of Multi Time-Delay

In this section we consider the system (Eq. 1) with MTDf. We restrict our analysis to the double-well case alone.

We choose $d = 0.5$, $\omega_0^2 = -1$, $\beta = 0.1$, $f = 0.1$, $\omega = 1$ and $\Omega = 10$. Figure 9 presents both theoretically and numerically computed Q as a function of the control parameter g for $L = 1, 2, 3$ and 5 for $\gamma = 0.3$ and for two values of α . The result for $\gamma = 0$ is also shown in this figure. VR is observed for all the values of L chosen. The theoretical Q value is in good agreement with the numerical Q value. In Fig. 9 two values of α are chosen in such a way that for one value $Q_{\max}(\gamma) > Q_{\max}(\gamma = 0)$ (the value of Q at resonance) while for the other value $Q_{\max}(\gamma) < Q_{\max}(\gamma = 0) = 2$.

Using the theoretical expression of Q , in $(\gamma - \alpha)$ parameter space we identify the regions where $Q_{\max}(\gamma) > Q_{\max}(\gamma = 0)$ for a few fixed values of L . The result is presented in Fig. 10. For both $\gamma < 0$ and $\gamma > 0$, Fig. 10 has L bands. In the bands filled with dots $Q_{\max}(\gamma) > Q_{\max}(\gamma = 0)$. The width of the bands is unequal.

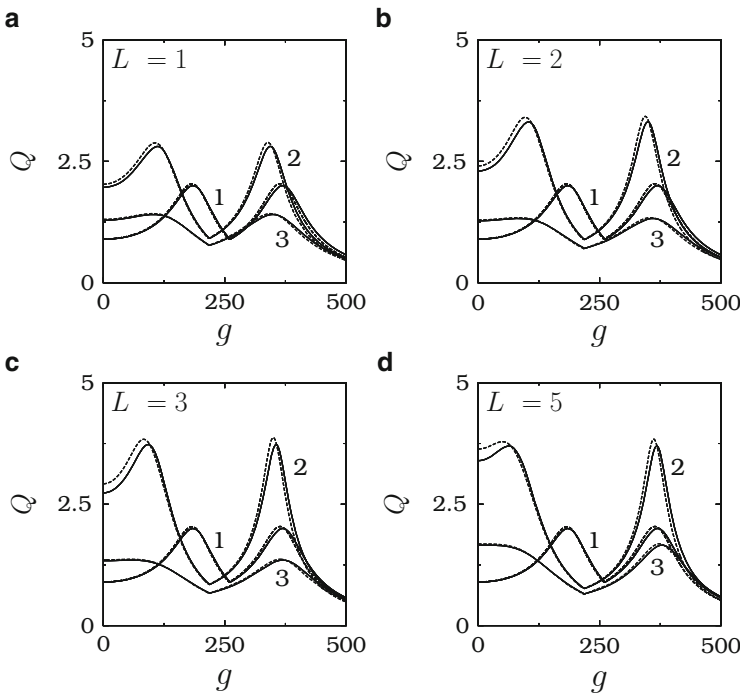


Fig. 9 Q versus g for a few fixed number of time-delayed feedback terms. We fixed $d = 0.5$, $\omega_0^2 = -1$, $\beta = 0.1$, $f = 0.1$, $\omega = 1$ and $\Omega = 10$. The *continuous and dashed lines* are the theoretically and numerically calculated values of Q , respectively. In all the subplots, $\gamma = 0$ for curve 1. For the curves 2 and 3 $\gamma = 0.3$ and $\alpha = 0.5$ and 5.5 , respectively

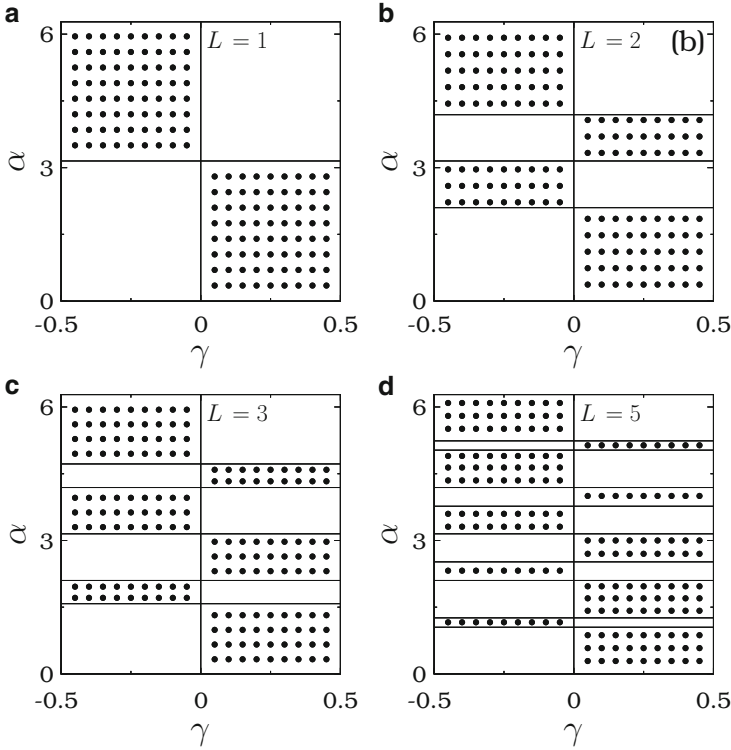


Fig. 10 Plot of regions (marked by dots) in the $(\gamma - \alpha)$ parameter space where $Q_{\max}(\gamma, \alpha) > Q_{\max}(\gamma = 0)$ for $\omega = 1$

The filled bands of $\gamma < 0$ become the unfilled bands of $\gamma > 0$. From the theoretical expression of Q the condition for the enhanced response at resonance due to the time-delayed feedback term is $\gamma \sum_{l=1}^L \sin l\alpha\omega > 0$ (refer Eq. (16)) and is realized in the regions filled with dots in Fig. 10. For each value of L the total length of α intervals where $Q_{\max}(\gamma) > Q_{\max}(\gamma = 0)$ is $\approx \pi$.

We define $G = Q_{\max}(\gamma)/Q_{\max}(\gamma = 0)$ as the gain factor. Figure 11 shows the variation of G as a function of the parameters γ and α for few values of L . In this figure data with $G > 1$ alone is plotted. For wide ranges of α and γ the gain factor is > 2 , that is, the delay is able to increase the value of Q at resonance more than twice the value of Q in its absence. The addition of more and more delay terms decreases the maximum value of G . Moreover, it produces new regions with $G > 1$ in the $(\gamma - \alpha)$ parameter space and decreases the value of G to less than 1 in certain regions where $G > 1$ earlier.

The resonance condition given by Eq. (18) and the results of cases 1 ($\gamma < 0$) and 2 ($\gamma > 0$) presented in Sect. 5 for a single delay-time are applicable for the MTDF with $\gamma \cos \alpha\omega$ replaced by $(\gamma/L) \sum_{l=1}^L \cos l\alpha\omega$. We point out that in the system (Eq. 1), in absence of MTDF, there are two resonances for $2|\omega_0^2| > \omega^2$, while one for $2|\omega_0^2| < \omega^2$. With MTDF the number of resonances for $\gamma < 0$ depends on

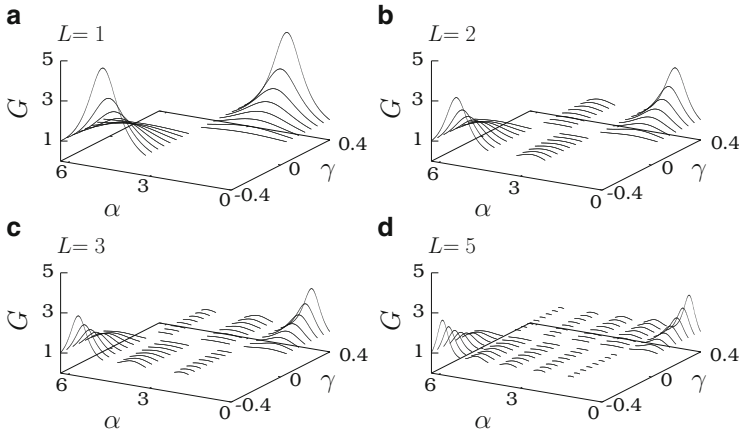


Fig. 11 $G = Q_{\max}(\gamma)/Q_{\max}(\gamma = 0) > 1$ versus γ and α for various values of L

the parameters ω , L and α . For $\gamma > 0$ the number of resonances depends also on the parameter ω_0^2 . Thus, by suitably choosing the values of γ , α and L the system can be set to show either two resonances or one resonance by varying the control parameter g . That is, the number of resonances can be varied by means of an MTDF.

In the single oscillator, an amplification of a low-frequency signal can be achieved for a range of amplitude and frequency of the high-frequency force in the absence of time-delayed feedback. In this case the maximum value of Q is $1/(d\omega)$. When the MTDF is introduced, we find $Q_{\max} = 1/|d\omega - (\gamma/L) \sum_{i=1}^L \sin i\alpha\omega|$. That is, Q_{\max} can be further increased or decreased by appropriate choices of γ , α and L . Thus, the MTDF can be used to control the value of Q_{\max} .

7 Signal Propagation in a System of n -Coupled Oscillators

In this section we focus our investigation on the signal propagation in a system of n -coupled Duffing oscillators, Eq. (2), with $n = 200$. In the system (Eq. 2) the external force is applied to the first oscillator alone. The coupling term is linear and has multiple time-delayed terms. The evolution of x_1 is independent of $x_i, i > 1$ while those of $x_i, i > 1$ depends on x_{i-1} .

7.1 Theoretical Approach

Writing $x_i = X_i + \psi_i$ where X_i 's and ψ_i 's are slow variables and fast variables, respectively, and applying the theoretical treatment used in Sect. 4, we obtain the following results:

$$Y_i(t) = Q_i f \cos(\omega t + \phi_i), \tag{26}$$

where

$$Q_1 = \frac{1}{\sqrt{(\omega_{r1}^2 - \omega^2)^2 + d^2\omega^2}}, \quad Q_i = P_i Q_{i-1}, \quad (27)$$

$$P_i = \frac{\delta r_\omega}{\sqrt{(\omega_{ri}^2 - \omega^2)^2 + d^2\omega^2}}, \quad i = 2, 3, \dots, n \quad (28)$$

$$\omega_{ii}^2 = C_i + 3\beta X_i^{*2}, \quad (29)$$

$$C_i = \omega_0^2 + \frac{3}{2}\beta\mu_i^2, \quad i = 1, 2, \dots, n \quad (30)$$

$$X_1^* \left(X_1^{*2} + \frac{C_1}{\beta} \right) = 0, \quad (31)$$

$$X_i^{*3} + \frac{C_i}{\beta} X_i^* - \frac{\delta}{\beta} X_{i-1}^* = 0, \quad i = 2, 3, \dots, n \quad (32)$$

$$\mu_1 = g/k, \quad \mu_i = \frac{\delta r_\Omega}{k} \mu_{i-1}, \quad i = 2, 3, \dots, n \quad (33)$$

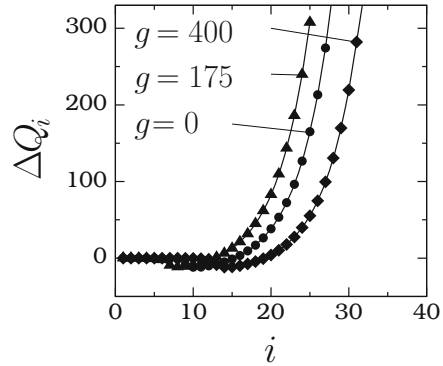
$$k = \sqrt{(\Omega^2 - \omega_0^2)^2 + d^2\Omega^2}, \quad (34)$$

$$r_\omega = \frac{1}{L} \left[\left(\sum_{l=1}^L \sin l\alpha\omega \right)^2 + \left(\sum_{l=1}^L \cos l\alpha\omega \right)^2 \right]^{1/2} \quad (35)$$

and r_Ω is similar to r_ω with ω replaced by Ω in Eq.(35). The above theoretical treatment gives an important result. When the number of time-delayed terms in the coupling is only one ($L = 1$), then $r_\omega = r_\Omega = 1$ and hence the response amplitudes Q_i 's, $i > 2$ are independent of the time-delay parameter α . This is because when $L = 1$ the coupling term $\delta x_{i-1}(t-\alpha)$ becomes $\delta X_{i-1}^* + \delta Q_{i-1} f \cos(\omega t - \alpha\omega + \phi_{i-1})$ in which $-\alpha\omega + \phi_{i-1}$ is an unimportant phase factor as far as the amplitudes of oscillation of x_i 's are concerned. The above theoretical prediction is verified in the numerical simulation. Therefore, in the rest of our analysis we consider $L > 1$.

In obtaining the theoretical Q_i , we have neglected the nonlinear terms in the equations of motion of ψ and $Y (= X - X^*)$. In the systems of n -coupled oscillators, the error in the theoretical Q due to the above approximation is found to be large for $i \gg 1$. To show this we define $\Delta Q_i = Q_{i,T} - Q_{i,N}$, where $Q_{i,T}$ and $Q_{i,N}$ represent Q_i values determined theoretically and numerically. In Fig. 12 we plot ΔQ_i with i for three values of g . For first few oscillators $\Delta Q_i \approx 0$ and then it diverges with i . In obtaining μ_i given by Eq. (33) we assumed that $\ddot{\psi}_i \gg \psi_i^2$ and ψ_i^3 . This can be a valid assumption for $i = 1$, where the first oscillator is driven by the high-frequency force $g \cos \Omega t$. Because the other oscillators are not driven explicitly by the high-frequency force, the assumption $\ddot{\psi}_i \gg \psi_i^2$ and ψ_i^3 is not valid for $i \gg 1$. Further, nonlinear terms in the equations of Y_i are neglected in obtaining Q_i . Moreover, the

Fig. 12 Variation of ΔQ_i (difference between the theoretically calculated Q_i and the numerically computed Q_i) with i for $d = 0.5, \omega_0^2 = 1, \beta = 1, f = 0.1, \omega = 1.5, \Omega = 15, L = 2, \delta = 2.5, \alpha = 1$ and for three values of g



errors in ψ_i and Y_i propagate to the $(i + 1)$ th oscillator through the coupling term. Consequently, ΔQ_i is negligible for the first few oscillators and becomes large for $i \gg 1$.

In order to minimize the error in the theoretical Q_i and also to reduce the propagation of this error through the consecutive oscillators, we include nonlinear terms in the calculation of the amplitudes of oscillation of the fast and slow variables [18]. We assume

$$\psi_i = \mu_i \cos(\Omega t + \phi_i), \quad X_i = A_i \cos(\omega t + \theta_i). \tag{36}$$

Substitution of (Eq. 36) in the equations

$$\begin{aligned} \ddot{\psi}_1 + d \dot{\psi}_1 + \omega_0^2 \psi_1 + \beta \psi_1^3 &= g \cos \Omega t, \\ \ddot{\psi}_i + d \dot{\psi}_i + \omega_0^2 \psi_i + \beta \psi_i^3 &= \frac{\delta}{L} \sum_{l=1}^L \psi_{i-1}(t - l\alpha), \end{aligned} \tag{37}$$

$$\begin{aligned} \ddot{X}_1 + d \dot{X}_1 + \omega_0^2 X_1 + \beta X_1^3 &= f \cos \omega t, \\ \ddot{X}_i + d \dot{X}_i + \omega_0^2 X_i + \beta X_i^3 &= \frac{\delta}{L} \sum_{l=1}^L X_{i-1}(t - l\alpha), \end{aligned} \tag{38}$$

where $i = 2, 3, \dots, n$ and $\omega_0^2 = \omega_0^2 + \frac{3}{2}\beta\mu_j^2, \quad j = 1, 2, \dots, n$ gives [65]

$$\mu_i^6 + a_\mu \mu_i^4 + b_\mu \mu_i^2 - R_{i\mu} = 0, \tag{39}$$

$$A_i^6 + a_{iA} A_i^4 + b_{iA} A_i^2 - R_{iA} = 0, \quad i = 1, 2, \dots, n \tag{40}$$

where

$$a_\mu = \frac{8}{3\beta} (\omega_0^2 - \Omega^2), \quad b_\mu = \frac{16}{9\beta^2} [(\omega_0^2 - \Omega^2)^2 + d^2 \Omega^2], \tag{41}$$

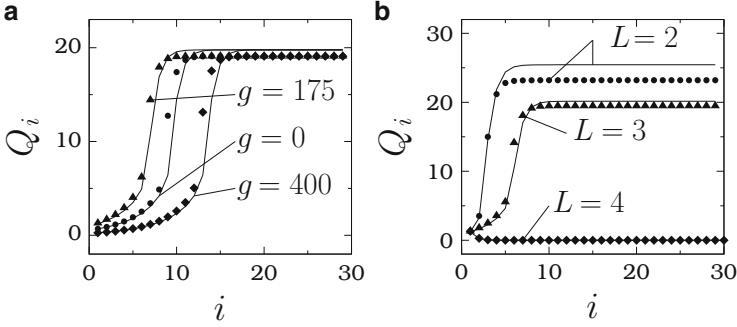


Fig. 13 Variation of Q_i with i for (a) three values of g with $L = 2$, $\alpha = 1$ and $\delta = 2.5$ and (b) three values of L with $g = 175$, $\delta = 5$ and $\alpha = 1$. The *continuous lines* and the *symbols* represent the theoretical and numerically computed values of Q_i , respectively

$$R_{1\mu} = \frac{16g^2}{9\beta^2}, \quad R_{1A} = \frac{16f^2}{9\beta^2}, \quad (42)$$

$$a_{iA} = \frac{8}{3\beta} (\omega_{0i}^2 - \omega^2), \quad b_{iA} = \frac{16}{9\beta^2} [(\omega_{0i}^2 - \omega^2)^2 + d^2\omega^2], \quad i = 1, 2, \dots, n \quad (43)$$

$$R_{i\mu} = \frac{16\delta^2 r_\Omega^2 \mu_{i-1}^2}{9\beta^2}, \quad R_{iA} = \frac{16\delta^2 r_\omega^2 A_{i-1}^2}{9\beta^2}. \quad i = 2, 3, \dots, n. \quad (44)$$

r_ω is given by Eq.(35) and r_Ω is obtained from r_ω by replacing ω by Ω . Equations (39) and (40) can be viewed as cubic equations for the variables μ_i^2 and A_i^2 , respectively. Analytical expressions for the roots of the cubic equation of the form (Eq.39) are given in [66]. We determine μ_i , A_i and then $Q_i = A_i/f$ by solving the Eqs. (39) and (40). We use $Q_{200} > Q_1$ as the criterion for undamped and enhanced signal propagation in the coupled oscillators.

We check the validity of the theoretical approach. In Fig. 13a we plot both the theoretically calculated Q_i and the numerically computed Q_i as a function of i for three values of g with $L = 2$, $\alpha = 1$ and $\delta = 2.5$. We observe a very good agreement of the theoretical Q_i with the numerical Q_i .

7.2 Undamped and Damped Signal Propagations

In Fig. 13a for each fixed value of g , for sufficiently large i , Q_i attains a saturation value. The variation of Q_i with i displays a kink-like dependence. That is, there is a critical number of oscillators for obtaining the maximum response and this number depends on the control parameters. An interesting observation in Fig. 13a is that

$Q_i > Q_1$ for $i > 1$, even in the absence of a high-frequency force. This implies that a coupling alone is able to give rise to an enhanced undamped signal propagation in the coupled oscillators. Figure 13b shows the influence of the number of time-delay terms in the coupling on Q_i , where $g = 175$, $\alpha = 1$ and $\delta = 5$. For $L = 2$ and 3 an undamped signal propagation occurs while for $L = 4$ a damped signal propagation takes place.

We call the limiting or saturation value of Q_i as Q_L . Interestingly, we can determine μ_L , A_L and hence $Q_L = A_L/f$ from Eqs. (39) and (40), respectively. Substituting $\mu_i = \mu_{i-1} = \mu_L$ and $A_i = A_{i-1} = A_L$ for sufficiently large i in Eqs. (39) and (40) we obtain

$$\mu_L = 0, \quad \left\{ \frac{4}{3\beta} \left[\Omega^2 - \omega_0^2 \pm \sqrt{\delta^2 r_\Omega^2 - d^2 \Omega^2} \right] \right\}^{1/2} \tag{45}$$

and

$$A_L = 0, \quad \left\{ \frac{4}{3\beta} \left[\omega^2 - \omega_{0L}^2 \pm \sqrt{\delta^2 r_\omega^2 - d^2 \omega^2} \right] \right\}^{1/2}, \tag{46}$$

where $\omega_{0L}^2 = \omega_0^2 + \frac{3}{2}\beta\mu_L^2$. $A_L = 0$ and $\neq 0$ correspond to a damped and an undamped signal propagation, respectively. It is also possible to find out the condition on δ for undamped signal propagation. In Fig. 13 in all the examples of undamped signal propagation $Q_2 > Q_1$. This is further confirmed for a large set of parametric values. Therefore, we assume that if $Q_2 > Q_1$, then

$$Q_i \geq Q_{i-1} \geq \dots > Q_3 > Q_2 > Q_1. \tag{47}$$

For Q_1 and Q_2 very much satisfactory analytical expressions are given by Eq. (27) with $i = 2$. The condition for $Q_2 > Q_1$ is $P_2 > 1$, where

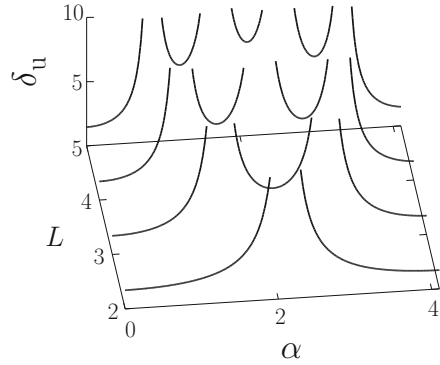
$$P_2 = \frac{\delta r_\omega}{\sqrt{(\omega_{r2}^2 - \omega^2)^2 + d^2 \omega^2}}, \quad \omega_{r2}^2 = \omega_0^2 + \frac{3\beta g^2 \delta^2 r_\Omega^2}{2\Omega^8}. \tag{48}$$

In this equation, $\omega_{r2}^2 \approx \omega_0^2$ because of $1/\Omega^8$ in the second term of ω_{r2}^2 . Then $P_2 > 1$ gives

$$\delta > \delta_u = \frac{\sqrt{(\omega_0^2 - \omega^2)^2 + d^2 \omega^2}}{r_\omega}. \tag{49}$$

Undamped signal propagation takes place for $\delta > \delta_u$. A very interesting result is that both Q_L and δ_u are independent of the amplitude g of the high-frequency periodic force. We can confirm this in Fig. 13a where numerically computed Q_i for different

Fig. 14 Dependence of δ_u on the time-delay α and the number of time-delayed terms L . $\delta_u < 10$ are alone shown in this plot



values of g approach the same limiting value. Figure 14 describes the dependence of δ_u on the number of time-delayed terms L and the time-delay α . In this figure, for clarity, only the values $\delta_u < 10$ are shown. When $\delta_u > 10$ is also considered then the δ_u curve has L peaks for a given value of L . For δ values above the threshold curve an undamped signal propagation occurs. For $L = 2$ and $\alpha = 1, 1.5$ and 3 the theoretical and the numerically computed values of δ_u are $(1.99, 1.96)$, $(3.38, 3.31)$ and $(2.32, 2.30)$, respectively. Figure 15 presents Q_L versus δ and α for four fixed values of L . In this figure we can clearly see the effect of the number of time-delayed terms L and the time-delay α on Q_L . The dependence of Q_L on α is nonmonotonic. Even for large values of δ there are intervals of α in which $Q_L = 0$ (damped signal propagation).

8 Conclusions

The role of the amplitude g of the high-frequency periodic force and the delay-time feedback parameters γ and α on VR is explored in the systems (Eqs. 1 and 2) through a theoretical approach. The theoretical treatment used in the present analysis allows us to predict the values of the control parameters at which resonance occurs, number of resonances, the maximum value of the response amplitude Q and explains the mechanism of resonance. The theoretical predictions of Q , g_{VR} and α_{VR} are in very good agreement with the numerical simulations. The presence of time-delay feedback is found to enrich the VR phenomenon. Particularly, the time-delay parameter α gives rise to a periodic or quasiperiodic pattern of VR profile. This feature of VR allows us to select different values (small or large) for the delay-time α to enhance the quality of the weak signal and it can be highly useful in optimizing the operation of multistable systems for the detection and regeneration of signals in a variety of experimental systems.

In the single oscillator, when the amplitude g of the high-frequency periodic force is varied, a single or a double resonance occurs depending upon the values

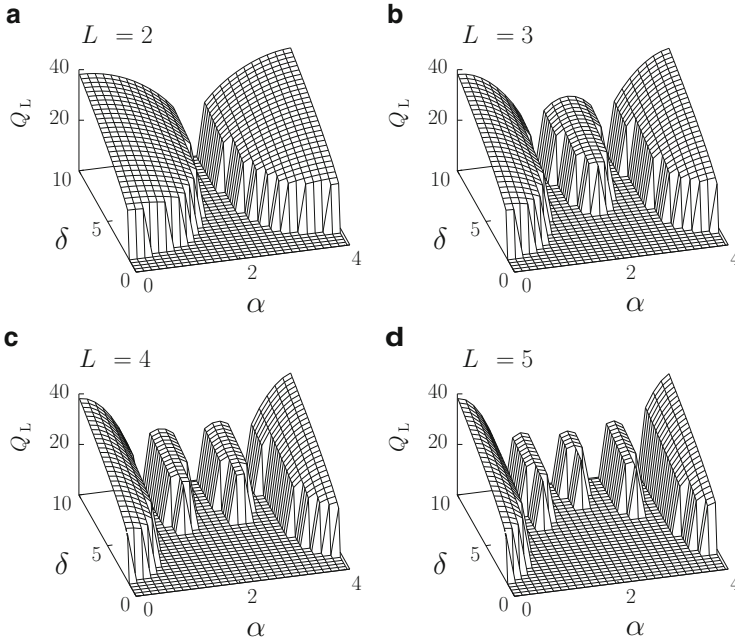


Fig. 15 Three-dimensional plot of Q_L versus δ and α for four fixed values of the number of time-delayed coupling terms L . Q_L is independent of the parameter g

of the parameters ω_0^2 , ω , α , L and γ and is independent of the parameters d , f , β and Ω . In the γ (the strength of feedback term)— α (time-delay) parameter space the regions with $Q_{\max}(\gamma) > Q_{\max}(\gamma = 0)$ have L bands where L is the number of time-delayed feedback terms. The maximum value of response amplitude is found to decrease when the number of feedback terms increases. The response amplitude Q depends on all the parameters except f (the analysis performed in the present work is valid only for $|f| \ll 1$) while its value at resonance depends on the parameters d , ω , γ , α and L .

More importantly, the theoretical approach is able to determine and explain the various features of signal propagation in coupled oscillators. One notable prediction is that in coupled oscillators the response amplitude as well as the dynamics is independent of the time-delay parameter α when the number of coupling terms is only one ($L = 1$). The system exhibits undamped signal propagation for appropriate choices of the parameters and these choices of parameters can be determined from the theoretical approach. We wish to stress that in the coupled oscillators system (2), even though only the first oscillator is driven by the high-frequency periodic force, fascinating results on signal propagation are obtained by the action of the unidirectional coupling with multiple time-delayed terms.

Acknowledgements MAFS acknowledges the financial support from the Spanish Ministry of Science and Innovation under Project No. FIS2009-09898.

References

1. Gammaitoni L, Hanggi P, Jung P, Marchesoni F (1998) *Rev Mod Phys* 70:223
2. McDonnell MD, Stocks NG, Pearce CEM, Abbott D (2008) *Stochastic resonance*. Cambridge University Press, Cambridge
3. Zambrano S, Casado JM, Sanjuan MAF (2007) *Phys Lett A* 366:428
4. Pikovsky AS, Kurths J (1997) *Phys Rev Lett* 78:775
5. Landa PS, McClintock PVE (2000) *J Phys Math Gen* 33:L433
6. Blekhman II, Landa PS (2004) *Int J Non Lin Mech* 39:421
7. Chizhevsky VN (2008) *Int J Bifurcat Chaos* 18:1767
8. Jeyakumari S, Chinnathambi V, Rajasekar S, Sanjuan MAF (2009) *Phys Rev E* 80:046608
9. Baltanas JP, Lopez L, Blekhman II, Landa PS, Zaikin A, Kurths J, Sanjuan MAF (2003) *Phys Rev E* 67:066119
10. Rajasekar S, Jeyakumari S, Chinnathambi V, Sanjuan MAF (2010) *J Phys Math Theor* 43:465101
11. Jeyakumari S, Chinnathambi V, Rajasekar S, Sanjuan MAF (2009) *Chaos* 19:043128
12. Rajasekar S, Abirami K, Sanjuan MAF (2011) *Chaos* 21:033106
13. Ullner E, Zaikin A, Garcia-Ojalvo J, Bascones R, Kurths J (2003) *Phys Lett A* 312:348
14. Yang JH, Zhu H (2012) *Chaos* 22:013112
15. Rajasekar S, Used J, Wagemakers A, Sanjuan MAF (2012) *Comm Nonlinear Sci Numer Simulat* 17:3435
16. Deng B, Wang J, Wei X, Tsang KM, Chan WL (2010) *Chaos* 20:013113
17. Jeevarathinam C, Rajasekar S, Sanjuan MAF (2013) *Ecol Complex* 15:33
18. Yao C, Zhan M (2010) *Phys Rev E* 81:061129
19. Yang JH, Liu XB (2011) *Phys Scripta* 83:065008
20. Chizhevsky VN, Giacomelli G (2008) *Phys Rev E* 77:051126
21. Atay FM (2010) *Complex time-delay systems: theory and applications*. Springer, Berlin
22. Lakshmanan M, Senthilkumar DV (2010) *Dynamics of nonlinear time-delay systems*. Springer, Berlin
23. Choe CU, Dahms T, Hovel P, Scholl E (2010) *Phys Rev E* 81:025205(R)
24. Fischer I, Vicente R, Buldu JM, Peil M, Mirasso CR, Torrent MC, Garcia-Ojalvo J (2006) *Phys Rev Lett* 97:123902
25. Vincente R, Gollo LL, Mirasso CR, Fischer I, Pipa G (2008) *Proc Natl Acad Sci USA* 105:17157
26. Flunkert V, D'Huys O, Danckaert J, Fischer I, Scholl E (2009) *Phys Rev E* 79:065201(R)
27. Ramana Reddy DV, Sen A, Johnston GL (2000) *Phys Rev Lett* 85:3381
28. Gassel M, Glatt E, Kaiser F (2007) *Fluct Noise Lett* 7:L225
29. Bonnin M, Corinto F, Gilli M (2007) *Int J Bifurcat Chaos* 17:4033
30. Dahlem MA (2009) *Phil Trans Roy Soc Lond* 367:1079
31. Yang JH, Liu XB (2010) *J Phys A Math Theor* 43:122001
32. Yang JH, Liu XB (2010) *Chaos* 20:033124
33. Jeevarathinam C, Rajasekar S, Sanjuan MAF (2011) *Phys Rev E* 83:066205
34. Hu D, Yang JH, Liu XB (2012) *Comm Nonlinear Sci Numer Simulat* 17:1031
35. Daza A, Wagemakers A, Rajasekar S, Sanjuan MAF (2013) *Comm Nonlinear Sci Numer Simulat* 18:411
36. Yang JH, Liu XB (2010) *Phys Scripta* 82:025006
37. Ahlborn A, Parlitz U (2005) *Phys Rev E* 72:016206
38. Shahverdiev EM, Shore KA (2008) *Phys Rev E* 77:057201

39. Gakkhar S, Negi K, Sahani SK (2009) *Comm Nonlinear Sci Numer Simulat* 14:850
40. Englert A, Kinzel W, Aviad Y, Butkovski M, Reidler I, Zigzag M, Kanter I, Rosenblum M (2010) *Phys Rev Lett* 104:114102
41. Englert A, Heiligenthal S, Kinzel W, Kanter I (2011) *Phys Rev E* 83:046222
42. Lee WS, Restrepo JG, Ott E, Antonsen TM (2011) *Chaos* 21:023122
43. Gakkhar S, Singh A (2012) *Comm Nonlinear Sci Numer Simulat* 17:914
44. Martinenghi R, Rybalko S, Jacquot M, Chembo YK, Larger L (2012) *Phys Rev Lett* 108:244101
45. Cushing JM (1977) *Integro-differential equations and delay models in population dynamics*. Springer, Berlin
46. Maza D, Mancini H, Boccaletti S, Genesio R, Arecchi FT (1998) *Int J Bifurcat Chaos* 8:1843
47. Khrustova N, Vesper G, Mikhailov A, Imbühl R (1995) *Phys Rev Lett* 75:3564
48. Schanz M, Pelster A (2003) *Phys Rev E* 67:056205
49. Larger L, Goldgebuier J, Erheux T (2004) *Phys Rev E* 69:036210
50. Erneux T, Glorieux P (2010) *Laser dynamics*. Cambridge University Press, Cambridge
51. Argyris A, Syvridis D, Larger L, Annovazzi-Lodi V, Colet P, Fischer I, Garcia-Ojalvo J, Mirasso CR, Pesquera L, Shore KA (2005) *Nature* 438:343
52. Uchida A, Amano K, Inoue M, Hirano K, Naito S, Someya H, Oowada I, Kurashige T, Shiki M, Yoshimori S, Yoshimura K, Davis P (2008) *Nat Photon* 2:728
53. MacDonald N (1989) *Biological delay systems: linear stability theory*. Cambridge University Press, Cambridge
54. Hashemi M, Valizadeh A, Azizi Y (2012) *Phys Rev E* 85:021917
55. Suel GM, Garcia-Ojalvo J, Liberman LM, Elowitz MB (2006) *Nature* 440:545
56. Mergenthaler K, Engbert R (2007) *Phys Rev Lett* 98:138104
57. Cabrera JL, Milton JG (2002) *Phys Rev Lett* 89:158702
58. Bauer S, Brox O, Kreissl J, Sartorius B, Radziunas M, Sieber J, Wunsche HJ, Henneberger F (2004) *Phys Rev E* 69:016206
59. Gerstner W, van Hemmen JL (1993) *Phys Rev Lett* 71:312
60. Bacci A, Huguenard JR, Prince DA (2003) *J Neurosci* 23:859; (2006) *Neuron* 49:119
61. Diez-Martinez O, Segundo JP (1983) *Biol Cybern* 47:33
62. Pakdaman K, Vibert JF, Boussard E, Azmy N (1996) *Neural Network* 9:797
63. Kane DM, Shore KA (2005) *Unlocking dynamical diversity: optical feedback effects on semiconductor lasers*. Wiley, New York
64. Shahverdiev EM, Shore KA (2008) *Phys Rev E* 77:057201
65. Jeevarathinam C, Rajasekar S, Sanjuan MAF (2013) *Chaos* 23:013136
66. Pipes LA, Harvill LR *Applied mathematics for engineers and physicists*, 3rd edn. McGraw-Hill, New York